한국해양공학회 2006년도 추계학술대회 논문집 pp. 420~425

Adaptive Stereoscopic-PIV System for the Analyses of the Flow-Structure-Interactions(FSI) of Air-Lifted Bodies

DEOG-HEE DOH*, TAE-GYU HWANG**, HYO-JE JO***, KENJI TANAKA**** AND MASAHIRO TAKEI*****
*Korea Maritime Univ., School of Mech. & Information Eng., Busan, Korea
**Georgia Inst. of Tech., Dept. of Mech. Eng.
***Korea Maritime Univ., Div. of Ocean Systems Eng.
****Okamoto Co. Ltd.
*****Nihon Univ., Dept. of Mech. Eng.

공기부양 물체의 유동-구조 연동운동 해석을 위한 능동형 스테레오-PIV 시스템

도덕희* · 황태규** · 조효제*** · Tanaka, K**** · Takei, M*****
*한국해양대 기계정보공학부
**Georgia Inst. of Tech., Dept. of Mech. Eng.
***한국해양대, 해양시스템공학부
****Okamoto Co. Ltd.
*****Nihon Univ., Dept. of Mech. Eng.

KEY WORDS: Swirl flow 선회유동, Floating cylinder 부유체실린더, Adaptive stereoscopic-PIV 능동형스테레오 PIV, Flow-structure interactions 유체-구조 연성

ABSTRACT: *Measurements results of flow-structure-interactions (FSI) of an air-lifted body are introduced. An adaptive stereoscopic-PIV system has been constructed for the measurements of the air-lifted body. The measurement system consists of two cameras and optical sensors. The flow characteristics around a lifted cylinder body(length=60mmm, diameter =10mm, polystyrene) in the swirling flow field in a vertical pipe (length=600mm, inner diameter=) are investigated by the use of the constructed adaptive stereoscopic-PIV system. The images of the two cameras were used for the analysis of the flow fields around the floated cylinder body. The images of the cylinder body captured by the two cameras were used for the analyses of its motions. Four optical sensors (LED) were used for the detection of the postures of the freely-lifted cylinder body. The FSI analyses have been carried out to find the physical conditions at which the floating body is stabilized with its upright postures.*

1. Introduction

Pneumatic conveyance systems have been widely adopted for transportations of industrial materials (Klinzing et al., 1997) and are more important in ocean application such as in risers. However they have problems of deterioration of the material quality due to collisions of the materials to the pipe wall, further low transportation efficiency. Studies on pneumatic conveyance systems with swirl flows have been performed with goals of avoiding the deterioration of the material quality. Li and Tomida(2000) investigated the flow characteristics of the polyethylene particles and polyvinyl ones to report the pressure drops in a horizontal pipe. However, their results were restricted to spherical materials. In some practical applications, the material that should be conveyed are cylindrical or complex shapes such as ocean minerals. The cylindrical materials moving in the swirling flow has a characteristic that its axis is orientated to the main flow direction in a certain flow condition. It was shown that the stable orientation of the cylindrical body to the main flow could be attained by using a swirling flow (Gould et al., 1983).

Horii et al. (1989) used a special swirling flow which had a steep axial velocity profile with swirling motion in order to transport particles without touching the inner wall, which resulted in a high performance transportation of the cylindrical materials. These studies are mainly focusing on the orientation efficiency. And there are few studies that report the flow characteristics around the cylindrical material body. Yin et al. (2003) reported a theoretical study on the force balances acting on a cylinder material in a swirl flow. Unfortunately, experimental investigations have not been reported on the flow characteristics around the rotating cylindrical material in a swirling flow.

제1저자 도덕희 연락처: 부산시 영도구 동삼동 한국해양대
051-410-4364 doh@mail.hhu.ac.kr

The purpose of the present study is to provide experimental investigation results on the flow characteristics around a cylindrical body floated in a vertical swirl flow and on the motional information of the body itself through constructions of a new 'Adaptive Stereoscopic-PIV system'.

2. Adaptive Stereoscopic PIV System

2.1 Hardwares

The adaptive stereoscopic-PIV system has been constructed to measure the flow characteristics around the cylindrical body which is floated freely by the swirl flow in a vertical pipe. The polystyrene cylinder (lc = 60 mm, dc = 10 mm, density 220 kg/m3) has been used as the cylinder body. Fig. 1 (a) shows the concept of the adaptive stereoscopic-PIV system. Four-LED-sensor unit detects the light reflected from the surface of the floating body, and it activates the conventional stereoscopic-PIV system when the cylinder body passes through the sensing zone in nearly vertical posture. The sensor unit is composed of four reflection type fiber sensors. The sensor unit were embedded in the pipe wall as shown in Fig. 1(b). The laser light sheet used for flow visualization around the body passes through the same vertical line of the sensor array. The red LED frequency is 680 nm.

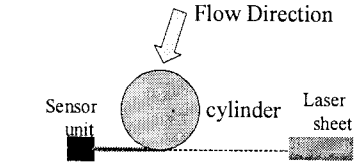

(a) location of sensing zone

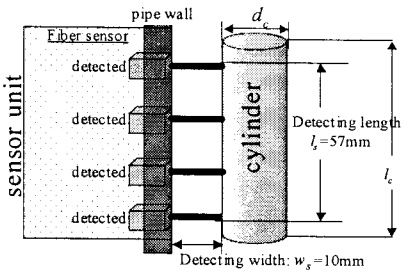

(b) oriented posture

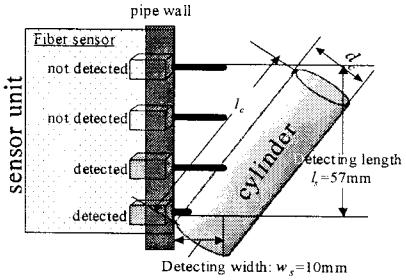

(b) non-oriented posture

Fig. 1 Adaptive sensing system

Fig. 1(b) shows the condition at which all four fiber sensors(OMRON, E3X-NA11F) detect the reflected lights from the cylinder body, which indicates the cylinder body floated and rotated by the swirl flows in the pipe is in upright condition (posture). The length of the sensor unit ls = 57 mm almost corresponds to the length of the rotating cylinder, lc = 60 mm. Fig. 1(c) shows the condition at which only two fiber sensors detect the cylinder body, which means the cylinder body rotates inside of the pipe with non-oriented posture (unstable). In the non-orientated case, the sensor unit does not activate the stereoscopic-PIV system. Since the response time of the fiber sensor was 20μs which is small enough than the body's collapsing time, the PIV system could be always activated adaptively in the same posture of the body without a fail. The detection length of the sensor unit has been adjusted to w_s = 10 mm from the pipe inner wall to attain maximum light signals reflected.

2.2 Softwares

In this study, a hybrid stereoscopic-PIV is used. The hybrid stereoscopic-PIV introduces, a geometric transformation to consider the refraction and the aberration of the lens and the camera calibration method used for the 3D-PTV measurement developed by Doh et al. (2004). In order to attain three-dimensional measurement with two cameras, it is necessary to know their camera parameters. The ten-parameter method (Doh et al., 2004) is used. Since the arrangement of the cameras has a large view angle, the obtained images are strongly distorted, which makes the camera calibration difficult. To overcome this matter, a two-dimensional image transformation on each camera image: warping, is carried out before using the original images for the camera calibration as shown in Eq. (1).

$$x = \frac{a_{11}x_s + a_{12}y_s + a_{13}}{a_{31}x_s + a_{32}y_s + 1}$$

$$y = \frac{a_{21}x_s + a_{22}y_s + a_{23}}{a_{31}x_s + a_{32}y_s + 1} \quad (1)$$

x, y : coordinates before transformation

xs, ys: coordinates after transformation

The calibrator image before and after transformation shown in Figs. 2 and 3. In this study, the image at the center physical plane (Z = 0 mm) was used to calculate the elements of the a_{ij} matrix.

In the ten-parameter method, 10 parameters (6 exterior parameters: l, α, β, γ, m_x, m_y, four interior parameters: c_x, c_y, k_1, k_2) are obtained. (α, β, γ) represents the tilting angles of the photographic coordinates axes against the absolute axes. Fig. 4 shows a coordinate relation when the photographical axes is set parallel to the absolute coordinate by tilting the angles (α, β, γ) . (X, Y, Z) represents the absolute coordinate, and (x, y, z) repre-

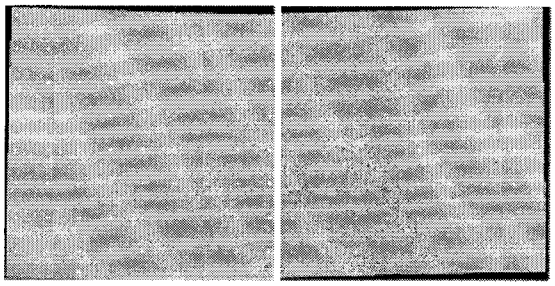

(a) camera 1 (b) camera 2

Fig. 2 Calibrator image before transformation

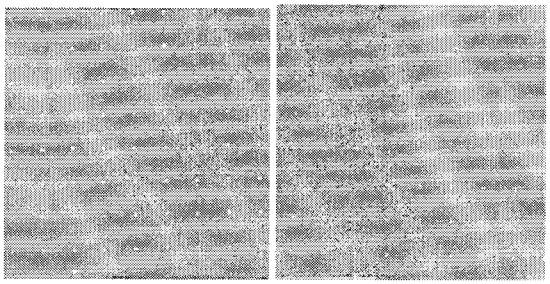

(a) camera 1 (b) camera 2

Fig. 3 Calibrator image after transformation

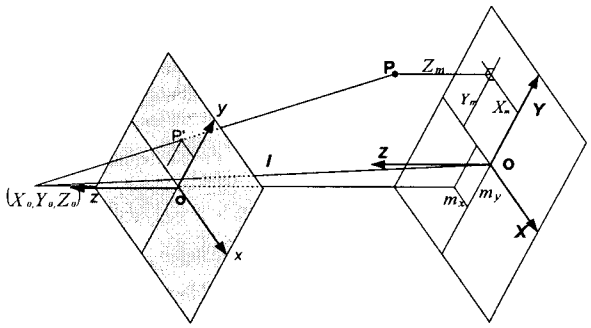

Fig. 4 The camera parameters on the absolute coordinate and the photographical coordinate

sents the photographical coordinate of the image centroid of the calibration targets. l means the distance between the origin O (0, 0, 0) and the principal point (X_0, Y_0, Z_0) of the camera.

The coordinate (X_m, Y_m, Z_m) represents the point P position of the calibrator when the camera coordinate is rotated with the tilting angles to make the collinear set in one line as shown in Fig. 4. The m_x and m_y means the point at which the normal vector from the origin O (X_0, Y_0, Z_0) of the camera coordinate meets with the X-Y plane. The collinear equation for every point between the two coordinates is expressed as Eq. (2). The c_x and c_y are the focal distances for x and y components of the coordinate. Δx and Δy are the lens distortions as expressed as Eq. (3). The Eq. (2) can be converted to the following Eq. (4)

Since this equation is a strong non-linear, an improved

$$x = c_x \frac{X_m - m_x}{\sqrt{dis^2 - m_x^2 - m_y^2 - Z_m}} + \Delta x$$
$$y = c_y \frac{Y_m - m_y}{\sqrt{dis^2 - m_x^2 - m_y^2 - Z_m}} + \Delta y \qquad (2)$$

$$\Delta x = \frac{x}{r}(k_1 r^2 + k_2 r^4), \quad \Delta y = \frac{y}{r}(k_1 r^2 + k_2 r^4)$$
$$r = \sqrt{x^2 + y^2} \qquad (3)$$

$$F = c_x \frac{X_m - m_x}{\sqrt{dis^2 - m_x^2 - m_y^2 - Z_m}} - (x - \Delta x) = 0$$
$$G = c_y \frac{Y_m - m_y}{\sqrt{dis^2 - m_x^2 - m_y^2 - Z_m}} - (y - \Delta y) = 0 \qquad (4)$$

Gauss-Newton calculation method (Kobayashi et al., 1989) is adopted to obtain all necessary parameters using the above two equations in Eq. (4). Once all camera parameters are obtained, the relations between the photographic coordinate and the absolute coordinate of the target image or the particle image can be expressed as the following Eq. (5). Where, MM is the matrix for the rotational transformation is expressed in the form of Eq. (6)

$$\begin{bmatrix} X \\ Y \\ Z \end{bmatrix} = M_M^{-1} \begin{bmatrix} X_m \\ Y_m \\ Z_m \end{bmatrix} = B \begin{bmatrix} X_m \\ Y_m \\ Z_m \end{bmatrix} \qquad (5)$$

$$X_m = \frac{x - \Delta x}{c_x} t + m_x$$
$$Y_m = \frac{y - \Delta y}{c_y} t + m_y \qquad (6)$$
$$Z_m = d - t$$

The camera center (X_0, Y_0, Z_0) can be expressed as Eq. (7), and the collinear equation for one target P (or particle P) can be expressed as P(X, Y, Z) = ($a_1 t + X_0$, $a_2 t + Y_0$, $a_3 t + Z_0$).

$$X_0 = B_{11} mx + B_{12} my + B_{13} d$$
$$Y_0 = B_{21} mx + B_{22} my + B_{23} d \qquad (7)$$
$$Z_0 = B_{31} mx + B_{32} my + B_{33} d$$

The cross-sectional points constructed from the following two collinear Eq. (8) for the two cameras are defined as the three-dimensional positions in the absolute coordinate.

$$A(X, Y, Z) = A(a_{11} t + b_{11}, a_{12} t + b_{12}, a_{13} t + b_{13})$$
$$B(X, Y, Z) = B(a_{21} s + b_{21}, a_{22} s + b_{22}, a_{23} s + b_{23}) \qquad (8)$$

Where, t and s are obtained by the least square method (LSM). Since the cross-sectional points do not always intersect on one

point, the below Eq. (9) is used for the definition of the last three-dimensional position of the targets (or the particles), which implies the center of the shortest distance between the two collinear equations.

$$\begin{bmatrix} X_P \\ Y_P \\ Z_P \end{bmatrix} = \frac{1}{2} \left\{ \begin{bmatrix} X_A \\ Y_A \\ Z_A \end{bmatrix} + \begin{bmatrix} X_B \\ Y_B \\ Z_B \end{bmatrix} \right\} \quad (9)$$

Where, X_A, Y_A and Z_A represent the absolute coordinates for camera A defined by Eq. (7). X_B, Y_B and Z_B represent the absolute coordinates for camera B. After obtaining the positions of the vector grid points (vector start points), the three-dimensional vector terminal points are calculated by combining the two-dimensional vector terminals of each camera's image. The two-dimensional vectors are obtained by the conventional gray level cross-correlation method (Kimura et al., 1986)

3. Experimental System and Procedures

Fig. 5 shows the overall measurement system. Two digital cameras (Kodak ES1.0, 1k x 1k) were used for the stereoscopic measurements and arranged as seen in the figure. Smoke (Glycol , d=0.5~ 1μm)was used as seeding particles and it was let into the main pipe (D=100mm, L=1100mm). Nd-Yag laser (120mJ, 15Hz) was used for flow field visualizations. The swirl flow is generated by suctioning the main pipe air at top with a blower. The air inlet is made at the bottom of the main pipe through four small horizontal pipes (d=10mm) as seen in the Fig. 5. As mentioned previously the floating body was put into the swirl flow field in order to investigate the flow properties at which its posture becomes upright rotating at a certain height from the bottom of the main pipe with stability. Its posture was sensed by the four optical sensors (LED, reflection type) attached on the pipe wall.

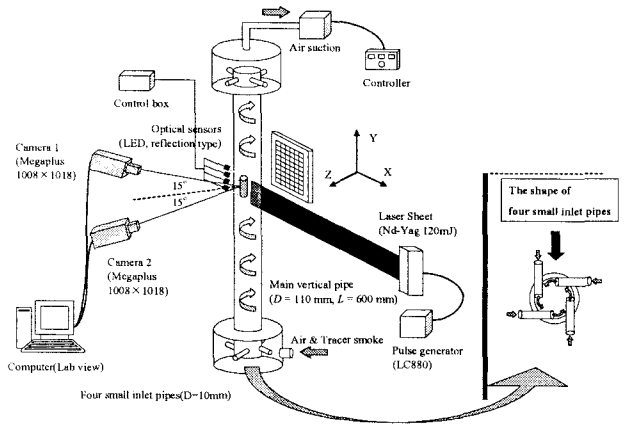

Fig. 5 Overall experimental system

Table 1 Four experiments were tested

Blowing condition	Suction condition
- Floating cylinder in	- Floating cylinder in
- Floating cylinder out	- Floating cylinder out

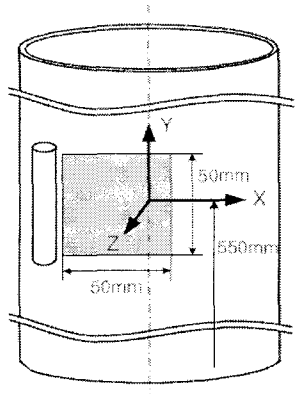

Fig. 6 Measurement region

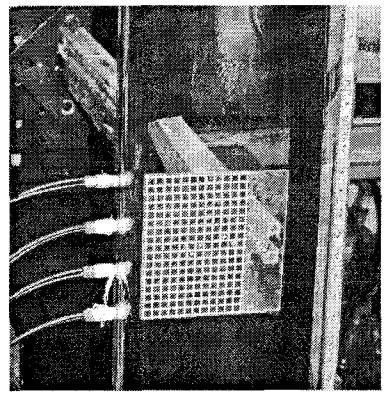

Fig. 7 Camera calibrator

The height of the cylinder's rotating position of the cylinder were controlled by adjusting the blower's speed control system. Four cases were tested as seen in the Table 1. Blowing condition implies that the flow was generated by the blower installed at the inlet of the main pipe. On the contrary, suction condition implies the blower was installed at the outlet of the main pipe. The flow rate was controlled by the blower's speed control using the motor inverter of the blower. The flow rate was maintained at 1.7×10^{-3} m^3/sec. The flow rate was measured with a flow meter installed at the outlet of the main pipe. The Reynolds number with the diameter of the main pipe is about 4240. Fig. 6 shows the measurement region. X is the horizontal direction of the vertical pipe. Y is the vertical direction of the vertical pipe. And Z is the azimuthal direction of the vertical pipe. The measured velocity components U, V and W were defined as the horizontal, vertical and azimuthal components, respectively. The measured velocities were normalized with the velocity obtained from the flow rate, 0.42m/sec. Before commencing the main experiments the camera calibration was carried out. A flat plate (56mm x

48mm) was attached onto a traverse and was moved to 9 positions to Z-axis direction (-12mm, -9mm, -6mm, -3mm, 0mm, 3mm, 6mm, 9mm, 12mm) with 3mm distance at which the images of the plate were captured for camera calibration. Fig. 7 shows the camera calibrator.

4. Results and Discussions

Fig. 8 shows a picture taken at an instance when the floating cylinder was maintained at a stable but not passing through the measurement zone. Fig. 9 shows instantaneous raw images taken by the two cameras in Fig. 5. Fig. 10 shows mean three-dimensional vector field. The number of instantaneous vector fields for averaging is 96. Every instantaneous vector field was obtained at the time when the bar came into the same posture regions. That is, an adaptive sampling for vector field was carried out and averaging was made at the same condition where the rotating bar comes into a certain area in the swirl flow. The two spots seen at the lower part in Fig. 10 are error vectors due to reflections. Fig. 11 shows the horizontal velocity profiles when the flow is blowing condition with the floating cylinder in and out conditions. There is a slight discrepancy between the two profiles even if the flow rate were maintained at the same. This is due to the existence of the floating cylinder. When the floating cylinder is rotating inside of the main pipe, W component increased along the whole radial direction.

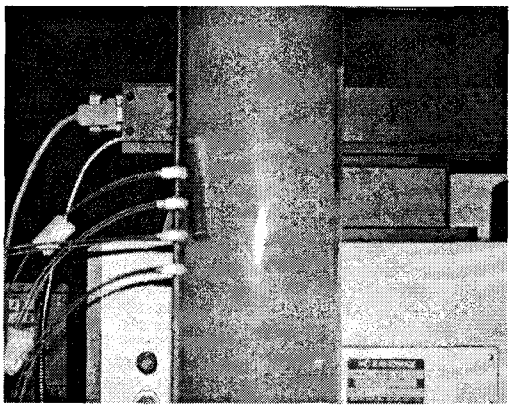

Fig. 8 Experimental picture taken at an instance

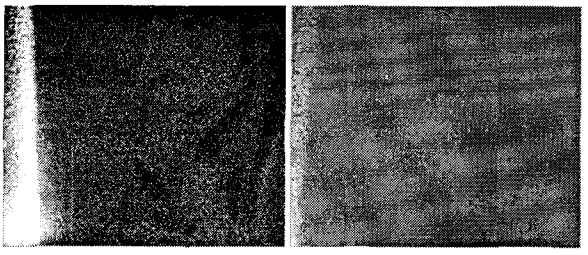

(a) viewed by camera 1 (b) viewed by camera 2

Fig. 9 Instantaneous raw image

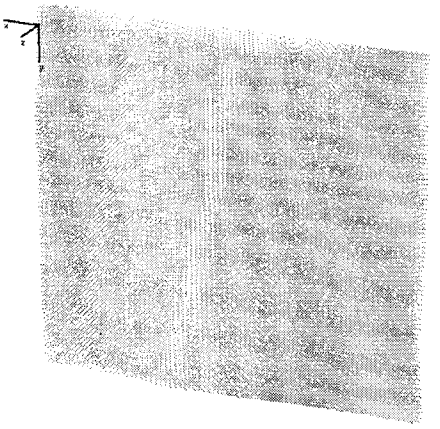

Fig. 10 Mean velocity field(Blowing with no floating cylinder)

V component that is a vertical component direction becomes decreased from x/R=0.3 to the floating cylinder's location while U component is still maintained in this region except the region over x/R=0.75. Fig. 12 shows the vertical velocity profile at x/R=0.8, which means the location of nearest vertical line along the floating cylinder. U, V and W components decreased along the whole zone except y/R=-0.1~0.05 for W component.

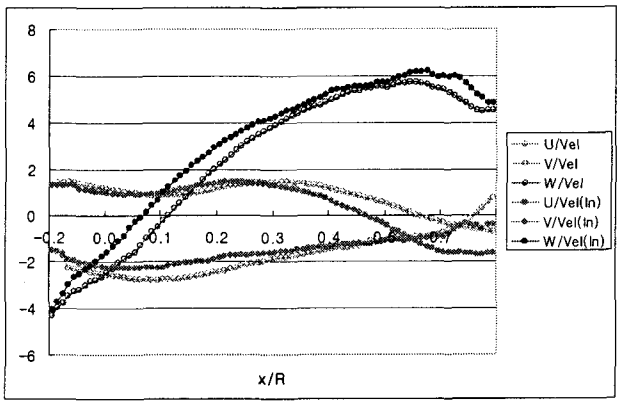

Fig. 11 Horizontal velocity profile at y/R=0.0(blowing condition)

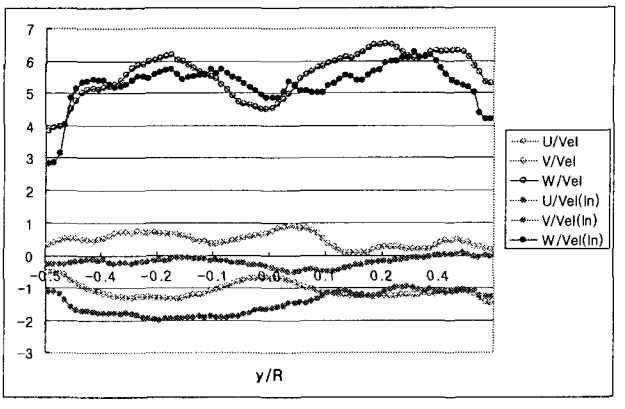

Fig. 12 Vertical velocity profile x/R=0.8 (blowing condition)

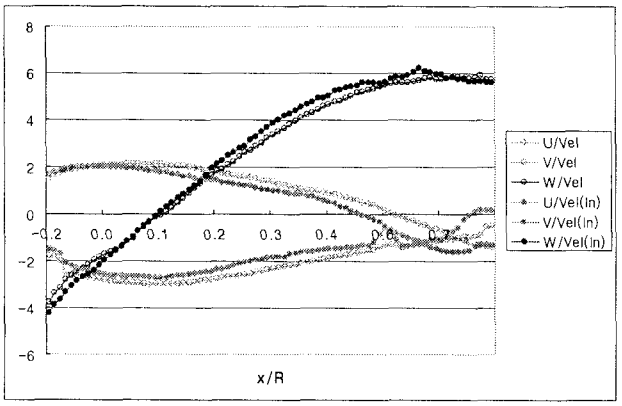

Fig. 13 Horizontal velocity profile at y/R=0.0(suction condition)

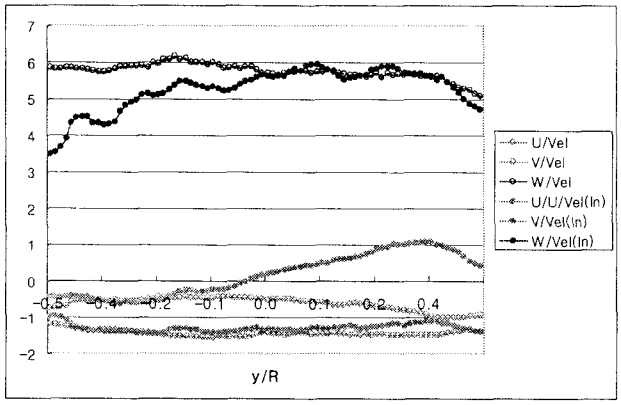

Fig. 14 Vertical velocity profile x/R=0.8(suction condition)

Fig. 12 shows the horizontal velocity profiles when the flow is suction condition with the floating cylinder in and out conditions. W components show similar profiles for both cylinder in and out conditions. U and V components shows decreased profiles over the whole x/R locations. Fig. 13 shows the vertical velocity profile at x/R=0.8 when suction condition. W component shows uniform profile showing different shape from that in the case of blowing. U, V and W components show homogeneous profiles along the whole y/R locations showing different profiles from those in the case of blowing, which implies that suction condition is better for maintaining the floating cylinder at stable posture during operation rather than the case of blowing.

5. Conclusion

An adaptive stereoscopic-PIV system has been developed for measuring the flow characteristics around the floating cylinder in a swirl flow.

It was seen that the height of the floating cylinder body was maintained at the same level regardless of blowing and suction conditions. For the case of suction, all velocity profiles of U, V, W are similar regardless of body in and out cases.

W component was dominant than other components and played crucial roles in stabilizing the posture of the floating body.

Turbulent properties were also investigated, but not mentioned this time, and it was seen that the turbulent properties were smaller in the case of suction than in blowing case, which implies that suction condition is better for controlling the floating cylinder than blowing condition, stable parallelization of the floating body. Further investigation to flow-structure interactions is now underway.

Acknowledgement

This work was supported by Korea Research Foundation (KRF-2006-521-D00078).

References

Adamczyk, A. A. and Rimai, L., (1988), "Reconstruction of a 3-dimensional flow field from orthogonal views of seed track video images", Experiments in Fluids, Vol.6, pp.380-386.

Doh, D.H, Hwang, T.G. and Saga, T., (2004), "3D-PTV measurements of the wake of a sphere", Measurement Science and Technology, Vol.15, pp.1059-1066.

Gould, I V, and Aust, M I E., (1983) "Vaccum-Pneumatic Conveying of Raw Wool", Mech., Eng. Trans., Vol.8, pp.77-83.

Horii, K., Matsumae, Y., Cheng, X.M, Takei, M. and Hashimo, B., (1989) "A Study of Spiral Flow (Part3) Opening and Orientation Control of Fiber by Spiral Flow", Trans. of the Japan Society for Aeronautical and Space Sciences, Vol.32, No.98, pp. 155-164.

Kimura, I., Takamori, T. and Inoue, T., (1986) "Image processing instrumentation of flow by using correlation technique", Journal of Flow Visualization and Image Processing, Vol. 6, No.22, pp.105-108.

Klinzing, E. G, Marcus D R, Rizk F, and Leung S. L, (1997), "Pneumatic conveying of solids", Chanpman & Hall, second edition, (1997).

Li, H. and Tomita, Y., (1994), "Characteristics of Swirling Flow in a Circular Pipe", Trans. ASME J. Fluid Engineering, Vol.116, No.2. pp.370-372.

Li, H. and Tomita, Y, (2000), "Particle Velocity and Concentration Characteristics in a Horizontal Dilute Swirling Flow Pneumatic Conveying", Powder Technology, Vol.107, pp.144-152.

Yin, C, Rosendahl, L, Kar, K. S. and Sorensen, H., (2003) "Modelling the motion of cylindrical particles in a nonuniform flow", Chemical Engineering Science, Vol.58, pp.3489-3498.